

Ionization energy based Fermi-Dirac statistics and its Lagrange multipliers

Andrew Das Arulsamy^{1, 2}

¹ Department of Physics, National University of Singapore, 2 Science Drive 3, Singapore 117542, Singapore

² Condensed Matter Group, No. 22, Jln Melur 14, Tmn Melur, Ampang, Selangor DE, Malaysia

(Dated: 10th December 2002)

Quantitative differences of Lagrange multipliers between standard Fermi-Dirac statistics (FDS) and Ionization energy (E_I) based FDS (iFDS) are analyzed in detail to obtain reasonably accurate interpretations without violating the standard FDS. The resistivity and Hall-resistance models in 1D, 2D and 3D are also derived to illustrate the transport phenomena in ferromagnetic manganites and superconducting cuprates. It is shown via simulation that the charge carriers in these materials seem to be strongly correlated in term of electron-ion attraction or simply, fermions in those materials are somewhat gapped due to Coulomb attraction. However, this model as will be pointed out, is not suitable for metals with free-electrons and strong electron-phonon coupling.

PACS numbers: 71.10.Ay, 72.10.Bg, 72.60.+g, 72.80.Ga

INTRODUCTION

Doped-compounds including oxides and its electrical and magnetic measurements have contributed enormously on the understanding of electrical properties of superconductors, ferromagnets and semiconductors. Two-dimensional (2D) E_I based Fermi liquid model was originally used to describe c -axis and ab -planes conduction of over-doped cuprate superconductors [1, 2]. Subsequently, it was further developed to capture both $T_{crossover}$ (c -axis pseudogap) and T^* (spin gap characteristic T) in ab -planes peculiar conduction involving spinons and holons which is known as the hybrid model [3, 4]. In this paper, iFDS is re-derived to extract the Lagrange multipliers so as to trigger sufficient interest for applications in other compounds specifically in ferromagnetic films and polycrystals above T_p (paramagnetic \leftrightarrow ferromagnetic transition T). $\rho(T)$ curves are simulated at various doping or gap (E_I) and T to further enhance its applicability specifically on La-Ca-Sr-Mn-O and Y-Ca-Ba-Cu-O compounds. In addition, it is also shown with detailed derivation of somewhat different Lagrange multipliers that separately influence the standard FDS and iFDS. Apart from that, the probability functions of electrons (e) and holes (h), charge carriers' concentrations, the resistivity and Hall-resistance models in 1D, 2D and 3D are derived as well via the standard quantum statistical method. Interpretations of electrical properties based on these models for manganites and some cuprates are also highlighted.

THEORETICAL DETAILS

Lagrange multipliers

The conduction e distribution can be derived using iFDS with ionization energy as an anomalous constraint. This derivation involves two restrictive conditions: (i)

the total number of e in a given system is constant and (ii) the total energy of n electrons in that system is also constant. Both conditions are as given below

$$\sum_i^\infty n_i = n, \quad (1)$$

$$\sum_i^\infty E_i n_i = E. \quad (2)$$

The condition as given in Eq. (2) can be rewritten as given below by inserting conditions, $E_{electron} = E_{initialstate} + E_I$ and $E_{hole} = E_{initialstate} - E_I$.

$$\sum_i^\infty (E_{initialstate} \pm E_I) n_i = E. \quad (3)$$

This is to justify that an e to occupy a higher state N from initial state M is more probable than from initial state L if condition $E_I(M) < E_I(L)$ at certain T is satisfied. As for a h to occupy a lower state M from initial state N is more probable than to occupy state L if the same condition above is satisfied. $E_{initialstate}$ is the energy of a particle in a given system at a certain initial state and ranges from $+\infty$ to 0 for e and 0 to $-\infty$ for h . The importance of this inclusion is that it can be interpreted as a gap that will be described later and also, particularly the E_I can be used to estimate the resistivity transition upon substitution of different valence state ions. By utilizing Eqs. (1) and (2), one can arrive at the probability functions in an explicit form as [2]

$$f_e(\mathbf{k}) = \exp \left[-\mu - \lambda \left(\frac{\hbar^2 \mathbf{k}^2}{2m} + E_I \right) \right], \quad (4)$$

Similarly, the probability function for h is given by

$$f_h(\mathbf{k}) = \exp \left[\mu + \lambda \left(\frac{\hbar^2 \mathbf{k}^2}{2m} - E_I \right) \right]. \quad (5)$$

The parameters μ and λ are the Lagrange multipliers. $\hbar = h/2\pi$, h = Plank constant and m is the charge carriers' mass. Note that E has been substituted with $\hbar^2 \mathbf{k}^2/2m$. In the standard FDS, Eqs. (4) and (5) are simply given by, $f_e(\mathbf{k}) = \exp[-\mu - \lambda(\hbar^2 \mathbf{k}^2/2m)]$ and $f_h(\mathbf{k}) = \exp[\mu + \lambda(\hbar^2 \mathbf{k}^2/2m)]$. Equation (1) can be rewritten by employing the 3D density of states (DOS) derivative, $dn = V \mathbf{k}^2 d\mathbf{k} / 2\pi^2$, that eventually gives [5]

$$n = \frac{V}{2\pi^2} e^{-\mu} \int_0^\infty \mathbf{k}^2 \exp \left[\frac{-\lambda \hbar^2 \mathbf{k}^2}{2m} \right] d\mathbf{k}, \quad (6)$$

$$p = \frac{V}{2\pi^2} e^\mu \int_{-\infty}^0 \mathbf{k}^2 \exp \left[\frac{-\lambda \hbar^2 \mathbf{k}^2}{2m} \right] d\mathbf{k}. \quad (7)$$

n is the concentration of e whereas p represents h 's concentration. V denotes volume in \mathbf{k} -space. The respective solutions of Eqs. (6) and (7) are given below

$$\mu_e = -\ln \left[\frac{n}{V} \left(\frac{2\pi \lambda \hbar^2}{m} \right)^{3/2} \right], \quad (8)$$

$$\mu_h = \ln \left[\frac{p}{V} \left(\frac{2\pi \lambda \hbar^2}{m} \right)^{3/2} \right]. \quad (9)$$

The subscripts e and h represent electrons and holes respectively. Separately, Eq. (2) can be written as

$$E = \frac{V \hbar^2}{4m\pi^2} e^{-\mu} \int_0^\infty \mathbf{k}^4 \exp \left(\frac{-\lambda \hbar^2 \mathbf{k}^2}{2m} \right) d\mathbf{k}. \quad (10)$$

Finally, one may obtain $\lambda_{FDS} = 1/k_B T$ after introducing $E = 3nk_B T/2$ [5], k_B is the Boltzmann constant. Applying the identical procedure to iFDS, i.e. by employing Eqs. (4) and (5), then Eqs. (6) and (7) are respectively rewritten as

$$n = \frac{V}{2\pi^2} e^{-\mu} \int_0^\infty \mathbf{k}^2 \exp \left(-\lambda \frac{\hbar^2 \mathbf{k}^2}{2m} - E_I \right) d\mathbf{k}, \quad (11)$$

$$p = \frac{V}{2\pi^2} e^\mu \int_{-\infty}^0 \mathbf{k}^2 \exp \left(\lambda \frac{\hbar^2 \mathbf{k}^2}{2m} - E_I \right) d\mathbf{k}. \quad (12)$$

The respective solutions of Eqs. (11) and (12) are

$$\mu + \lambda E_I = -\ln \left[\frac{n}{V} \left(\frac{2\pi \lambda \hbar^2}{m} \right)^{3/2} \right], \quad (13)$$

$$\mu - \lambda E_I = \ln \left[\frac{p}{V} \left(\frac{2\pi \lambda \hbar^2}{m} \right)^{3/2} \right]. \quad (14)$$

Note that Eqs. (13) and (14) simply imply that $\mu_e(iFDS) = \mu_e + \lambda E_I$ and $\mu_h(iFDS) = \mu_h - \lambda E_I$. Furthermore, using Eq. (3), one can rewrite Eq. (10) as

$$E = \frac{V \hbar^2}{4m\pi^2} e^{-\mu - \lambda E_I} \int_0^\infty \mathbf{k}^4 \exp \left(\frac{-\lambda \hbar^2 \mathbf{k}^2}{2m} \right) d\mathbf{k}, \quad (15)$$

As such, one can surmise that, λ remains the same, $1/k_B T$ that can be verified from Eqs. (13) and (15). I.e., $\lambda_{FDS} = \lambda_{iFDS}$ as required by the standard FDS. Hence, the relationship between FDS and iFDS in term of Lagrange multipliers has been derived and shown clearly.

Resistivity models

Denoting $\mu = E_F$ (Fermi level), $\lambda = 1/k_B$, $\hbar^2 \mathbf{k}^2/2m = E$ and substituting these into Eqs. (4) and (5) will lead one to write

$$f_e(E) = \exp \left[\frac{E_F - E_I - E}{k_B T} \right], \quad (16)$$

$$f_h(E) = \exp \left[\frac{E - E_I - E_F}{k_B T} \right]. \quad (17)$$

At this point, one might again wonder the reason for E_I 's inclusion. The unique reason is that it directly determines the kinetic energies of e which carry the identity of its origin atom. Detailed experimental implications are given in section 5. These iFDS probability functions for e and h are unique in a sense that it allows the prediction of charge carriers' concentrations at various T and doping. It is worth noting that, $-E_I$ in Eq. (17) for h follows naturally from the Dirac's theory of antiparticle interpretations [6]. Besides, the charge carriers are not entirely free since there exist a gap-like parameter that can be related to electrons-ion or Coulomb attraction. In fact, application of Eqs. (16) and (17) in c -axis of 2D superconductors are very well explained [1, 2, 3, 4]. The general equations to compute charge carriers' concentrations are stated below,

$$n = \int_0^\infty f_e(E) N_e(E) dE, \quad (18)$$

$$p = \int_{-\infty}^0 f_h(E) N_h(E) dE. \quad (19)$$

Existence of E_g , which is the energy gap due to energy band splitting or lattice based gap is not inserted explicitly thus it is (if any) coupled with E_I , which is tied to ions via Coulomb attraction. Having said that, now it is possible to obtain the geometric-mean concentrations of e and h for 1D, 2D and 3D respectively in the forms of (assuming $n \approx p$)

$$\sqrt{np}(1D) = \frac{(m_e^* m_h^*)^{1/4}}{\hbar} \sqrt{\frac{k_B T}{2\pi}} \exp \left[\frac{-E_I}{k_B T} \right], \quad (20)$$

$$\sqrt{np}(2D) = \frac{k_B T}{\pi \hbar^2} \sqrt{m_e^* m_h^*} \exp \left[\frac{-E_I}{k_B T} \right], \quad (21)$$

$$\sqrt{np}(3D) = 2 \left[\frac{k_B T}{2\pi \hbar^2} \right]^{\frac{3}{2}} (m_e^* m_h^*)^{\frac{3}{4}} \exp \left[\frac{-E_I}{k_B T} \right]. \quad (22)$$

The DOS, $N(E, 1D) = (E^{-1/2} \sqrt{m^*/2})/\pi\hbar$, $N(E, 2D) = m^*/\pi\hbar^2$ and $N(E, 3D) = (E^{1/2}/2\pi^2)(2m^*/\hbar^2)^{3/2}$ were employed in which, m^* is the effective mass. Consequently, the resistivity models for 1D, 2D and 3D can be derived from $\rho = m/ne^2\tau$ by taking $1/\tau = AT^2$. The respective $\rho(T, E_I)$ are given by

$$\rho(1D) = \frac{A_1 \hbar (m_e^* m_h^*)^{1/4}}{e^2} \sqrt{\frac{2\pi T^3}{k_B}} \exp \left[\frac{E_I}{k_B T} \right], \quad (23)$$

$$\rho(2D) = \frac{A_2 \pi \hbar^2}{e^2 k_B} T \exp \left[\frac{E_I}{k_B T} \right], \quad (24)$$

$$\begin{aligned} \rho(3D) = & \frac{A_3}{2e^2} \left[\frac{2\pi \hbar^2}{k_B} \right]^{-3/2} (m_e^* m_h^*)^{-3/4} \\ & \times \sqrt{T} \exp \left[\frac{E_I}{k_B T} \right]. \end{aligned} \quad (25)$$

Note that A_1 , A_2 and A_3 are T independent scattering rate constants in 1D, 2D and 3D respectively. τ denotes scattering rate due to e - e scattering in the absence of magnetic field, \mathbf{H} .

Hall resistance

The equations of motion (EOM) for charge carriers in ab -planes under the influence of static (\mathbf{H}) and electric

field (\mathbf{E}) can be written in an identical fashion as given in Ref. [7], which are given by

$$m \left[\frac{d}{dt} + \frac{1}{\tau_H} \right] v_b = -e\mathbf{E}_y + e\mathbf{H}_x v_z, \quad (26)$$

$$m \left[\frac{d}{dt} + \frac{1}{\tau_H} \right] v_x = e\mathbf{E}_x - e\mathbf{H}_z v_y. \quad (27)$$

The subscripts x , y and z represent the axes in x , y and z directions while the scattering rate, $\tau_H = A_{D=2,3}^H/T^2$ in which $A_{D=2,3}^H$ may not be necessarily equals to $A_{D=2,3}$, though both $A_{D=2,3}$ and $A_{D=2,3}^H$ are independent of T . The subscript D represents dimensionality while the superscript H denotes applied \mathbf{H} for Hall effect. In a steady state of a static \mathbf{H} and \mathbf{E} , $dv_z/dt = dv_y/dt = 0$ and $v_z = 0$ hence one can obtain

$$\mathbf{E}_z = -\frac{e\mathbf{H}_x \mathbf{E}_y \tau_H}{m}. \quad (28)$$

In addition, it is further assumed that $\rho_x(T) = \rho_y(T) = \rho_z(T) = \rho(T)$. $R_H^{(z)}$ is defined as $\mathbf{E}_z/j_y \mathbf{H}_x$, $j_y = \mathbf{E}_y/\rho(T)$ and $\tan \theta_H^{(z)} = \mathbf{E}_z/\mathbf{E}_y$. Parallel to this,

$$R_H^{(z)} = \frac{\tan \theta_H^{(z)} \rho(T)}{\mathbf{H}_x}. \quad (29)$$

j_y is the current due to charge carriers' motion along y -axis and $\theta_H^{(z)}$ is the Hall angle. Furthermore, one can rewrite $\tan \theta_H^{(z)}$ as equals to $-e\mathbf{H}_x/m\tau_H$. Therefore, one can easily surmise that $\cot \theta_H^{(z)} \propto T^2$. After employing Eqs. (24) and (25), then one can respectively arrive at

$$R_H^{(2D)} = -\frac{A_2 \pi \hbar^2}{(m_e^* m_h^*)^{1/2} A_2^{(H)} k_B} T^{-1} \exp \left[\frac{E_I}{k_B T} \right], \quad (30)$$

$$\begin{aligned} R_H^{(3D)} = & -\frac{A_3}{2A_3^{(H)} (m_e^* m_h^*)^{5/4}} \left[\frac{2\pi \hbar^2}{k_B} \right]^{-3/2} \\ & \times T^{-3/2} \exp \left[\frac{E_I}{k_B T} \right]. \end{aligned} \quad (31)$$

The negative charges in Eqs (28), (30) and (31) are due to the assumption that the charge carriers are electrons. Note that $R_H(T, 1D)$ for any given samples that exhibit purely 1D conduction is obviously irrelevant or simply, could not be derived with above procedures, since Hall effect requires at least 2D conduction. There are nowhere in this derivation that takes into account any free electrons and T -dependence of e -phonon scattering. Hence,

these models are obviously not suitable for such applications except for semiconducting free electrons above conduction band. In this case, Eqs. (18) and (19) should be integrated from $E_g \rightarrow \infty$ and $0 \rightarrow -\infty$ respectively after replacing $E_I = 0$ in Eqs. (16) and (17). As for free electrons with strong phonon contributions, it is advisable to switch to the well known Bloch-Grüneisen formula given by [8],

$$\rho(T, 3D) = \rho_0 + \lambda_{tr} \frac{128\pi m^*(k_B T)^5}{ne^2(k_B \Theta_D)^4} \times \int_0^{\Theta_D/2T} \frac{x^5}{\sinh^2 x} dx. \quad (32)$$

λ_{tr} = electron-phonon coupling constant, $\rho_0 = \rho(T = 0)$, m^* = average effective mass of the occupied carrier states, Θ_D = Debye temperature, n = free electrons concentrations. As a matter of fact, one should *not* be prompted to substitute any of the Eqs. (20), (21) and (22) for n into Eq. (32) just to capture the electron-phonon scattering because the scattering of free electrons considered in Eq. (32) could not be compatible with *gapped* electrons' scattering of iFDS.

DISCUSSION

Figures 1, 2 and 3 illustrates the variation of $\rho(T)$ from Eqs (23), (24) and (25) with conduction dimensionality and doping parameter (E_I). One can also identify the $\rho(T)$ transition from metallic \rightarrow semiconducting conduction (from curve c \rightarrow a) with increasing E_I . It is also worth noting that $\rho(T, 1D)$, $\rho(T, 2D)$ and $\rho(T, 3D)$ are $\propto T^{3/2}$, T and \sqrt{T} respectively if and only if $E_I \ll T$. Another point worth to extract from these curves are the relationship between $T_{crossover}$ and E_I , where $T_{crossover} < E_I$ for 1D, $T_{crossover} = E_I$ for 2D and $T_{crossover} > E_I$ for 3D. Apparently, these relations are again due to the proportionalities of $\rho(T, 1D) \propto T^{3/2}$, $\rho(T, 2D) \propto T$ and $\rho(T, 3D) \propto \sqrt{T}$. Figures 4 and 5 plots the simulated $R_H(T)$ curves in 2D and 3D as well as at different E_I (0 K, 150 K, 310 K) that follows from Eqs (30) and (31). There are no significant differences of R_H between 2D and 3D since $R_H(2D)$ and $R_H(3D)$ are \propto to T^{-1} and $T^{-3/2}$ respectively. Besides, the T from $\exp[E_I/T]$ also inversely proportional to both $R_H(2D)$ and $R_H(3D)$. These scenarios will always lead R_H to increase with lowering T without any observable $T_{crossover}$ regardless of E_I 's magnitude, unlike in $\rho(T)$. It is convenient to directly quantify $\rho(T)$ variation with doping by relating E_I as a doping parameter, as will be discussed in the following paragraph for both manganites and cuprates.

Manganites' electrical properties were first reported by Jonker and van Santen [9, 10]. They further suggested that ferromagnetism is due to indirect coupling of d -shells

via conducting e . Subsequently, Zener [11, 12], Anderson and Hasegawa [13] have provided sufficient theoretical backgrounds on Zener's Double Exchange (DE) mechanism. However, this paper will not discuss the property of DE mechanism below T_p , instead the electrical properties above T_p (paramagnetic phase) will be addressed in detail in which, DE mechanism is employed at $T < T_p$ (ferromagnetic phase). It is interesting to observe reduced $\rho(T)$ and increased Curie temperature (T_p) at higher \mathbf{H} for $\text{La}_{1-x}\text{Ca}_x\text{Sr}_x\text{MnO}_3$ compounds [14, 15, 16]. The results that larger \mathbf{H} giving rise to conductivity at $T \geq T_p$ point towards the enhancement of conductivity from DE where the exponential increase of $\rho(T)$ is suppressed with larger \mathbf{H} . Interestingly, Nagaev [17] argued that small or large polarons are negligible in La-Ca-Sr-Mn-O compounds based on dielectric constants. In addition, Moskvin [18, 19] reinforces the importance of considering different charge distribution in MnO_6 , Mn and Oxygen instead of just considering the DE mechanism. Parallel to this, doping-friendly resistivity models derived from iFDS will indeed lead to an identical conclusions of Nagaev and Moskvin since iFDS did not consider polarons and the substitution of Ca^{2+} or $\text{Fe}^{2+,3+,4+}$ into $\text{La}_{1-x}\text{Ca}_x\text{Mn}_{1-y}\text{Fe}_y\text{O}_3$ system does indeed modify the overall charge distribution in accordance with the valence state of Ca, La, Mn and Fe. Add to that, Louca and Egami [20] invoked the Jahn-Teller (JT) distortion to describe the effect of lattice in T_p . They have utilized the results of pulsed neutron-diffraction experiments to conclude that the variation in Mn-O bond length with Sr substitution in $\text{La}_{1-x}\text{Sr}_x\text{MnO}_3$ compound can be related to JT. Again, note here that the change of Mn-O length with Sr substitution implies the valence state of Mn varies with doping. In a simpler compound of $\text{La}_{1-x}\text{Ca}_x\text{MnO}_3$, substitution of Ca into La, will have to satisfy the inequality of average E_I between Ca^{2+} (867 kJmol^{-1}) and La^{3+} (1152 kJmol^{-1}) i.e., $E_I(\text{La}^{3+}) > E_I(\text{Ca}^{2+})$. Here, one can easily fix the valence state of Ca^{2+} and La^{3+} as noted. As a consequence, this will ease the prediction of $\rho(T)$ with doping. If one of the ions is multivalence, then the linear algebraic equation as given below must be used to predict the valence state of the multivalence ion from $\rho(T)$ curves [4].

$$\frac{\delta}{j} \sum_{i=z+1}^{z+j} E_{Ii} + \frac{1}{z} \sum_{i=1}^z E_{Ii} = \frac{1}{q} \sum_{i=1}^q E_{Ii}. \quad (33)$$

The first term, $\frac{\delta}{j} \sum_{i=z+1}^{z+j} E_{Ii}$ above has $i = z + 1, z + 2, \dots, z + j$ and $j = 1, 2, 3, \dots$. It is solely due to multivalence ion for example, assume $\text{Mn}^{3+,4+}$ is substituted with Nd^{3+} ($\text{La}_{0.7}\text{Ca}_{0.3}\text{Mn}_{1-x}\text{Nd}_x\text{O}_3$) hence from Eqs (33), the first term is due to Mn^{4+} ion's contribution or caused by reaction of the form $\text{Mn}^{3+} - \text{electron} \rightarrow \text{Mn}^{4+}$, hence j is equals to 1 in this case and δ represents the additional contribution from Mn^{4+} . The second ($i =$

1, 2, 3, ..., z) and last ($i = 1, 2, 3, \dots, q$) terms respectively are due to reaction of the form $\text{Mn} - 3(\text{electrons}) \rightarrow \text{Mn}^{3+}$ and $\text{Nd} - 3(\text{electrons}) \rightarrow \text{Nd}^{3+}$. Recall that $q = z = 3+$ and $i = 1, 2, 3, \dots$ represent the first, second, third, ... ionization energies while $j = 1, 2, 3, \dots$ represent the fourth, fifth, sixth, ... ionization energies. Therefore, $z + \delta$ gives the minimum valence number for Mn which can be calculated from Eq. (33).

As for cuprates, the effect of Nd^{3+} ($E_I = 1234 \text{ kJmol}^{-1}$) substitution into Sr^{2+} ($E_I = 807 \text{ kJmol}^{-1}$) in superconducting $\text{TiSr}_{2-x}\text{Nd}_x\text{CaCu}_2\text{O}_7$ compound [21] was found to increase the $\rho(T)$ in accordance with E_I . This justifies the need for E_I based analysis on doping as pointed out by iFDS. Applications of iFDS in superconductors are explicitly given in Refs. [1, 2]. Recently, Naqib *et al.* [22] have investigated the electrical properties of $\text{Y}_{1-x}\text{Ca}_x\text{Ba}_2(\text{Cu}_{1-y}\text{Zn}_y)_3\text{O}_{7-d}$ superconducting compounds by varying x, y and d . The transition of $\rho(T)$ with Ca^{2+} are in excellent agreement with Eq. (23) of iFDS. Zn^{2+} doping is not appropriate to analyze as a function of iFDS because this substitution will directly disturb the *ab*-plane conduction of spinons and holons and also in term of oxygen concentration (d), thus the overall conductivity of $\text{Y}_{1-x}\text{Ca}_x\text{Ba}_2(\text{Cu}_{1-y}\text{Zn}_y)_3\text{O}_{7-d}$ polycrystals will be modified in a not-so-simple way [3, 4]. It is easy however, to extract the relation of $\rho(T)$ between $\text{Y}_{0.9}\text{Ca}_{0.1}\text{Ba}_2\text{Cu}_3\text{O}_{7-d}$ and $\text{Y}_{0.8}\text{Ca}_{0.2}\text{Ba}_2\text{Cu}_3\text{O}_{7-d}$ where $\rho(T)$ is reduced with Ca^{2+} doping for all d (oxygen pressure), since $\text{Y}^{3+}(E_I = 1253 \text{ kJmol}^{-1}) > \text{Ca}^{2+}(E_I = 867 \text{ kJmol}^{-1})$. All E_I values were calculated from Ref. [23] and the predictions stated above are only valid for reasonably pure materials without any significant impurity phases as well as with minimal grain boundary effects.

CONCLUSIONS

Conclusively, the ionization energy based Fermi-Dirac statistics is useful to estimate the transitional progress of $\rho(T, \text{doping})$ from metallic \rightarrow semiconducting or vice versa in cuprates and manganites. This is made possible by an additional unique constraint, which is nothing but the ionization energy that captures the electrons kinetic energies and maps it to its origin atoms. The relation of Lagrange multipliers (λ, μ) between FDS and iFDS have been derived explicitly solely to flush-out any misinterpretations that will lead to further complications in describing experimental data on *c*-axis superconductors and ferromagnets. The presented iFDS model however, do not admit completely free-electrons and strong phonon dependence.

FIG. 1: Simulated $\rho(T)$ curves from Eq. (23) that captures 1D conduction at various E_I .

FIG. 2: Simulated $\rho(T)$ curves from Eq. (24) that captures 2D conduction at various E_I .

acknowledgments

ADA would like to thank the National University of Singapore for the financial aid and also Prof. Feng Yuan Ping for his support. The author also thanks Hendry Izaac Elim, Chong Kok Boon and Kostyantyn Zloschastyev for their kind help and especially Salleh H. Naqib for communicating some of the unpublished experimental data. The author is grateful to A. Innasimuthu, I. Sebastiammal, A. Das Anthony and Cecily Arokiam for their partial financial assistances.

[1] A. Das Arulsamy, *Physica C* **356** (2001) 62.
[2] A. Das Arulsamy, *Phys. Lett. A* **300** (2002) 691.
[3] A. Das Arulsamy, P. C. Ong, M. T. Ong, *Physica B* **325** (2002) 164.
[4] A. Das Arulsamy, [cond-mat/0206293](https://arxiv.org/abs/cond-mat/0206293).
[5] D. J. Griffiths, *Introduction to quantum mechanics*, (Prentice-Hall, Inc., New Jersey, 1995).
[6] J. J. Sakurai, *Advanced quantum mechanics*, (Addison-Wesley, Inc., USA, 1967).
[7] C. Kittel, *Introduction to solid state physics* (John Wiley and Sons Inc., New York, 5th Ed., 1976).
[8] J. J. Tu, G. L. Carr, V. perebeinos, C. C. Homes, M. Strongin, P. B. Allen, W. N. Kang, E. -M. Choi, H. -J. Kim, S. -I. Lee, *Phys. Rev. Lett.* **87** 277001 (2001).
[9] G. H. Jonker, J. H. van Santen, *Physica* **16**, 337 (1950).
[10] J. H. van Santen, G. H. Jonker, *Physica* **16**, 599 (1950).
[11] C. Zener, *Phys. Rev.* **81**, 440 (1951).
[12] C. Zener, *Phys. Rev.* **82**, 403 (1951).
[13] P. W. Anderson, H. Hasegawa, *Phys. Rev.* **100**, 675 (1955).
[14] Y. M. Mukovskii, A. V. Shmatok, *J. Magn. Magn. Mater.* **196-197**, 136 (1999).
[15] R. Mahendiran, R. Mahesh, A. K. Raychaudhuri, C. N. R. Rao, *Solid State Commun.* **94**, 515 (1995).
[16] A. Gupta, G. Q. Gong, G. Xiao, P. R. Duncombe, P. Lecoeur, P. Trouilloud, Y. Y. Wang, V. P. Dravid, J. Z. Sun, *Phys. Rev. B* **54**, 15629 (1996).
[17] E. L. Nagaev, *Physica B* **284-288**, 1426 (2000).
[18] A. S. Moskvin, *Physica B* **252**, 186 (1998).
[19] A. S. Moskvin, I. L. Avvakumov, *Physica B* **322**, 371 (2002).
[20] D. Louca, T. Egami, *Physica B* **241-243**, 842 (1998).
[21] R. Abd-Shukor, A. Das Arulsamy, *J. Phys. D* **33**, 836

FIG. 3: Simulated $\rho(T)$ curves from Eq. (25) that captures 3D conduction at various E_I .

FIG. 4: Simulated 2D curves of Hall resistance as in Eq. (30) at various E_I .

(2000).
[22] S. H. Naqib, J. R. Cooper, J. L. Tallon, C. Panagopoulus, **cond-mat**/0209457.
[23] <http://www.webelements.com>.

FIG. 5: Simulated 3D curves of Hall resistance as in Eq. (31) at various E_I .

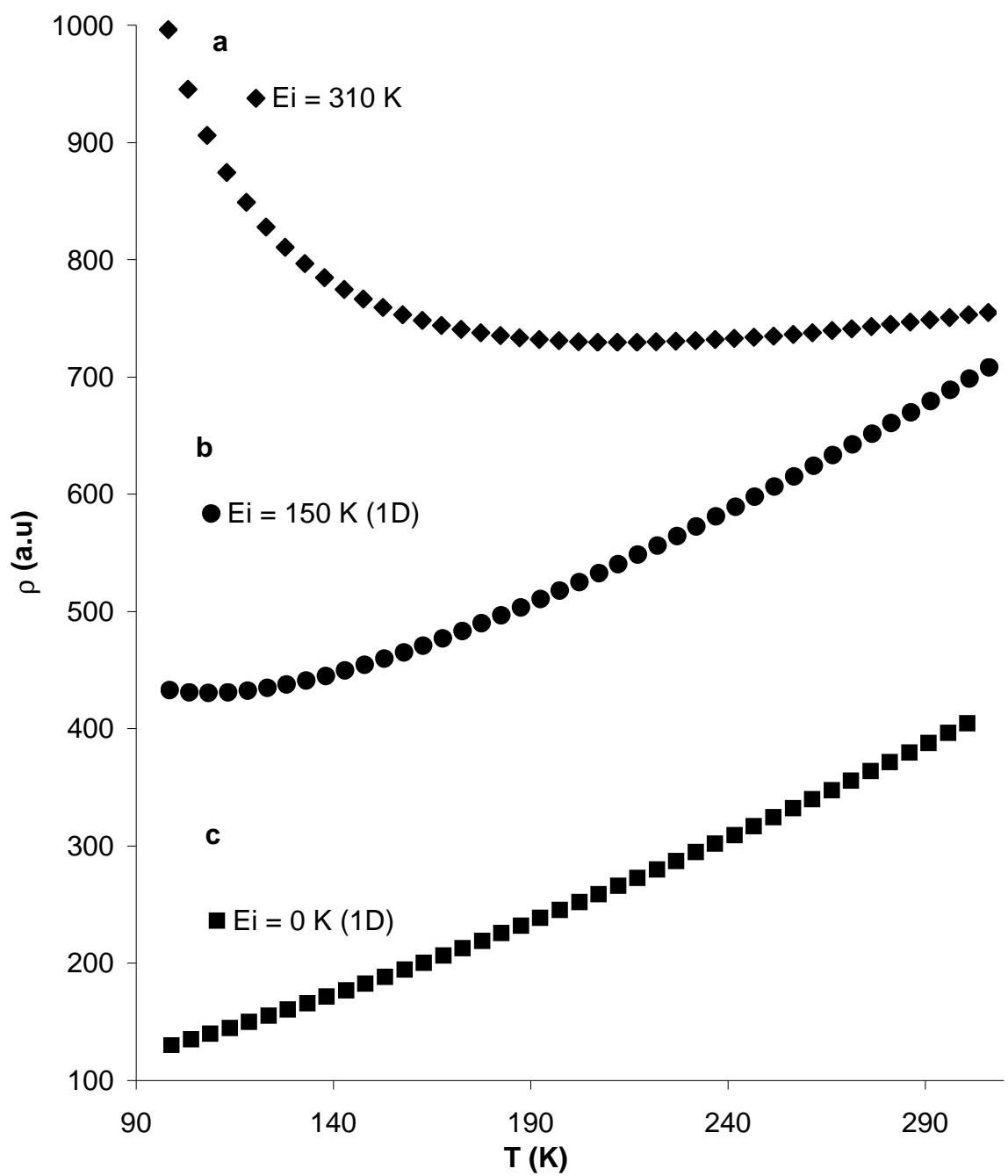


FIGURE 1 (A. D. Arulsamy)

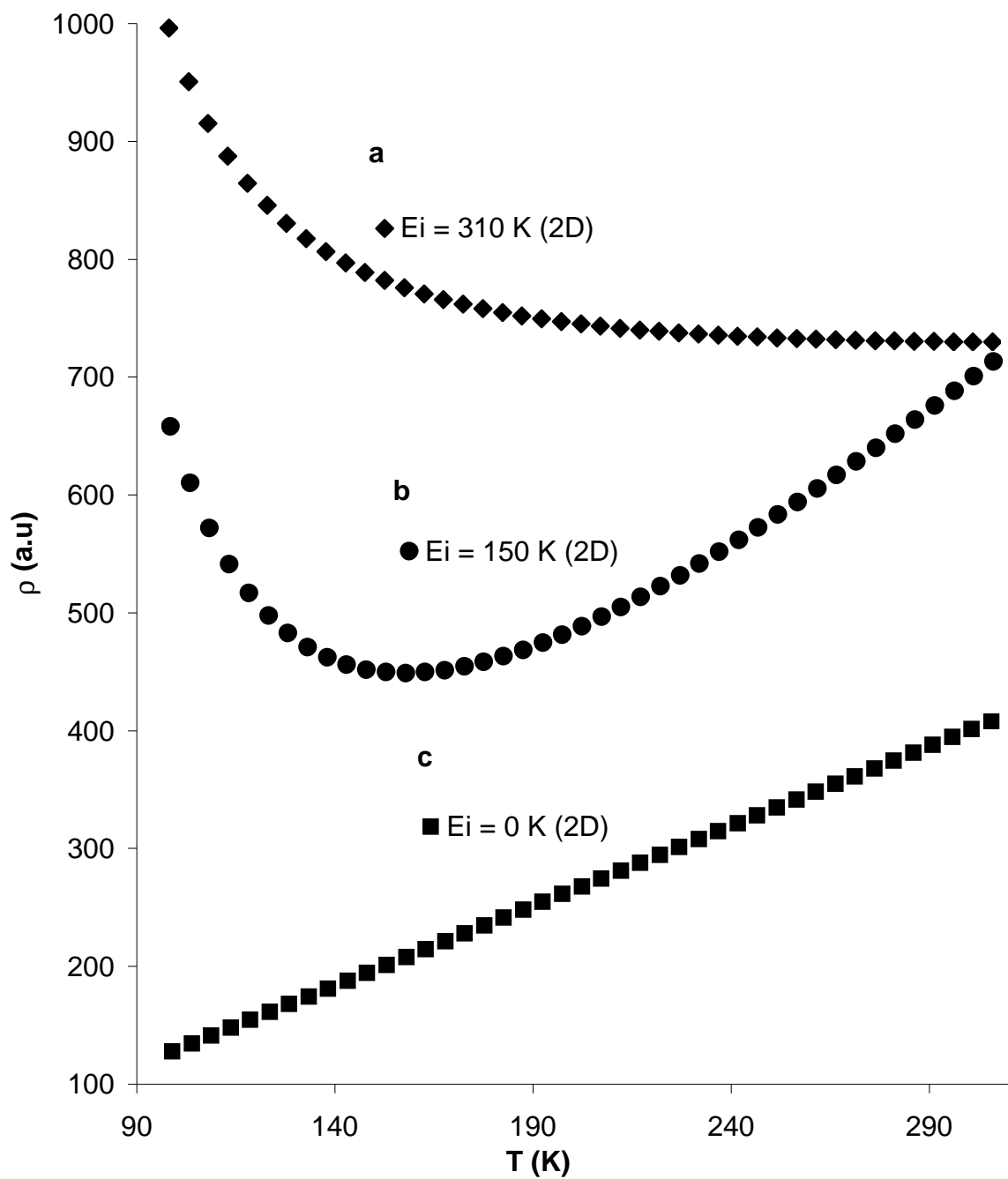


FIGURE 2 (A. D. Arulsamy)

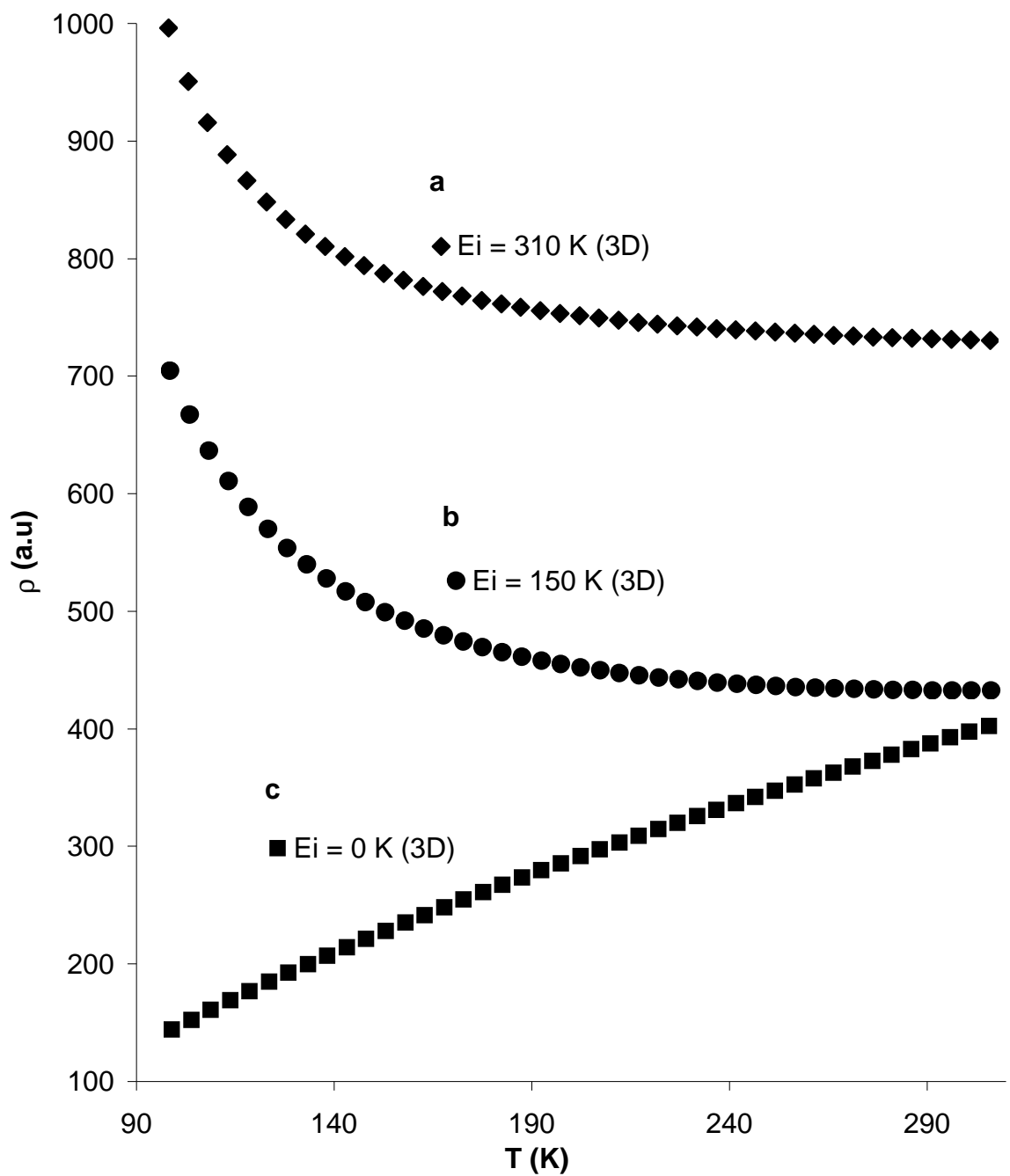


FIGURE 3 (A. D. Arulsamy)

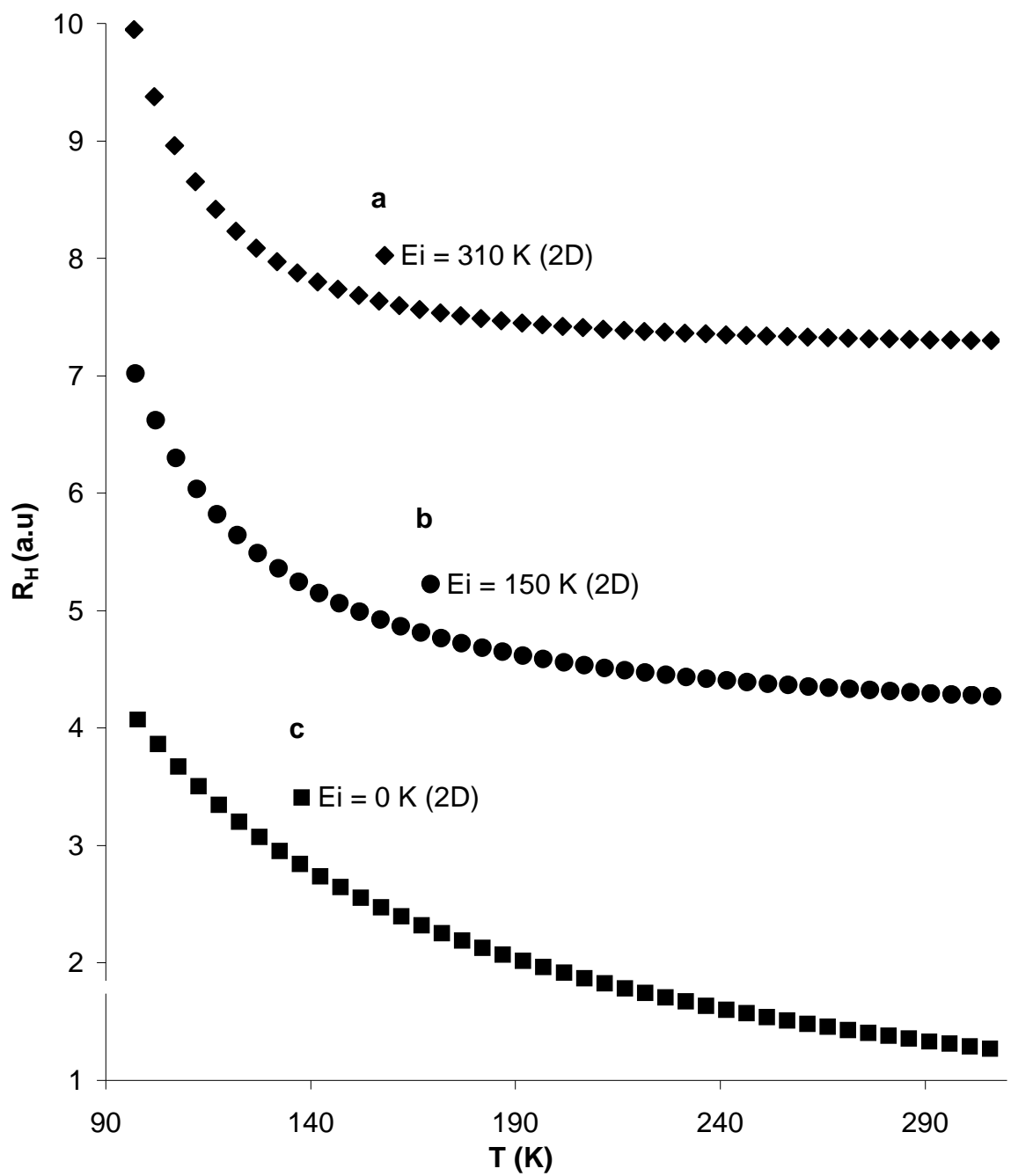


FIGURE 4 (A. D. Arulsamy)

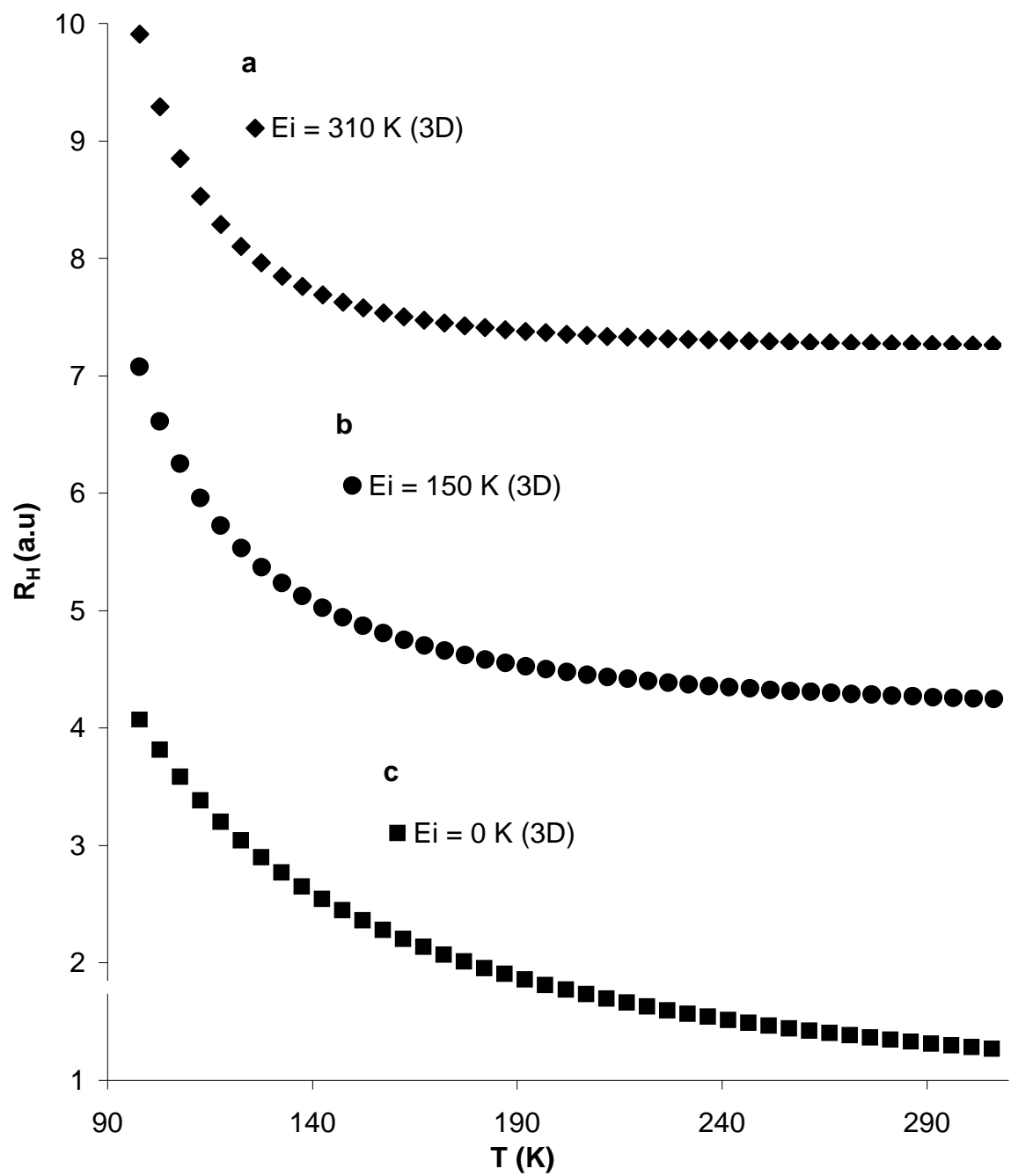


FIGURE 5 (A. D. Arulsamy)